




Cite this: *Chem. Commun.*, 2025, 61, 1136

Received 18th October 2024,  
Accepted 9th December 2024

DOI: 10.1039/d4cc05554c

rsc.li/chemcomm

# Synergistically stabilized SAPO-37-tetragonal zirconia composites: a promising catalyst for ethyl levulinate synthesis†

K. Khadheeja Shabana, Soumya B. Narendranath, N. P. Nimisha and  
A. Sakthivel \*

**A tetragonal zirconia-faujasitic SAPO-37 zeolite composite (SAP-37ZR) was synergistically stabilised at 550 °C using a temperature programmed reduction method. The presence of the zeolite-ZrO<sub>2</sub> composite phase was confirmed through powder XRD reflection, SEM and TEM-ED pattern analyses. The developed SAP-37ZR composite, exhibiting moderate acidity, was found to be highly active for the production of ethyl levulinate (EL) from furfuryl alcohol with a 99% yield.**

Silicoaluminophosphate (SAPO) based zeolite catalysts are well-known for their roles in dewaxing, methanol-to-olefin (MTO) conversion, and isomerization processes in the petroleum industry.<sup>1</sup> Compared to aluminosilicate-based zeolites, SAPOs are preferred due to their moderate acidity and strong resistance to coking. In this context, the faujasite-type SAPO-37, with its large supercages similar to those in fluid catalytic cracking (FCC) catalysts (such as ultrastable Y), is particularly promising for bio-refineries.<sup>2</sup> However, unlike zeolite Y, SAPO-37 suffers from poor structural stability due to P–O–P bond hydrolysis, which occurs when its  $\beta$ -cages are exposed to water molecules, leading to framework disintegration.<sup>3</sup> To address this, researchers have focused on enhancing the stability of the SAPO-37 framework by introducing hydrophobic environments through the introduction of organosilane,<sup>4</sup> metal–oxycarbide composites,<sup>5</sup> vapor-treatment,<sup>6</sup> etc.

Transition metals, their oxides, and clay-based catalysts have garnered significant attention in bio-refinery, and biomass conversion to platform molecules, etc., owing to their diverse physico-chemical properties.<sup>7,8</sup> To address non-renewable fossil fuel issues, biofuels are extracted from biomass, especially lignocelluloses, which can be hydrolyzed into platform compounds like furfuryl alcohol (FA) and levulinic acid. FA alcoholysis produces alkyl levulinates, which are promising fuel additives

due to their high lubricity, low sulfur content, and superior flow properties.<sup>8</sup> In this regard, it is worth mentioning that zirconia (ZrO<sub>2</sub>) exists in various forms, with meta-stable tetragonal zirconia (t-ZrO<sub>2</sub>) being particularly recognized as a promising green catalyst for numerous organic transformations.<sup>9</sup> The presence of anionic species such as sulfate,<sup>10</sup> phosphate,<sup>11</sup> or dopants like Y<sub>2</sub>O<sub>3</sub><sup>12</sup> aids in stabilizing tetragonal zirconia (t-ZrO<sub>2</sub>), making it suitable for several chemical processes, including syngas conversion<sup>13</sup> and methanethiol synthesis.<sup>14</sup> Encapsulating t-ZrO<sub>2</sub> within confined environments, such as mesoporous silica or zeolites, enhances its acid–base and redox properties, thereby broadening its application scope.<sup>15,16</sup> Introducing a zirconium source into the SAPO-37 matrix through post-synthetic methods, followed by heating under a hydrogen atmosphere (temperature programmed reduction), facilitates the encapsulation of ZrO<sub>2</sub> in the supercages of SAPO-37. This process helps to stabilize the tetragonal phase of ZrO<sub>2</sub> while preserving the SAPO-37 framework by maintaining surface hydrophobicity.

The resulting tetragonal zirconia-SAPO-37 composite (SAP-37ZR) has proven to be a promising catalyst for the preparation of ethyl levulinate (EL), ethylfurfuryl ether, and  $\gamma$ -valerolactone (GVL), which are valuable as fuel additives, flavoring agents, and transportation fuels. The inherent properties of the SAP-37ZR catalyst enable tuning of the selectivity of EL and furfuryl ether by simply adjusting the reaction temperature.

All the chemicals were used in their received form. The parent SAPO-37 material was synthesized using a hydrothermal method following the reported procedure.<sup>4</sup> The parent SAPO-37 is represented as SAPO-37as, the SAPO-37 sample treated with zirconium isopropoxide is labelled as SAP-37Z and those obtained by subsequent reduction are represented as SAP-37ZR. The synthesized materials were systematically characterized and explored for ethyl levulinate synthesis from furfuryl alcohol (FA). The details of the experimental procedures are summarised in the ESI.†<sup>17</sup>

The calcination of the as-prepared SAPO-37 leads to structural collapse and the formation of an amorphous phase due to the water molecules trapped in the  $\beta$ -cages.<sup>3</sup> The SAP-37ZR

*Inorganic Materials & Heterogeneous Catalysis Laboratory, Department of Chemistry, School of Physical Sciences, Central University of Kerala, Tejaswini Hills Kasaragod, 671316 Kerala, India. E-mail: sakthivelcuk@cukerala.ac.in*

† Electronic supplementary information (ESI) available: Experimental details, Fig. S1–S16. See DOI: <https://doi.org/10.1039/d4cc05554c>

developed in the present studies exhibits framework vibrational bands (Fig. S1, ESI†) even after TPR treatment at 550 °C, supporting the encapsulation of  $t\text{-ZrO}_2$  in the channel and cage of faujasite SAPO-37 to enable framework stability. The functional groups and framework vibration of SAP-37ZR were followed by FTIR spectral studies and showed characteristic vibrational bands at 529 and 558  $\text{cm}^{-1}$  attributed to the double six-membered ring (D6R) of the faujasite-type SAPO-37. A strong T–O–T (T = Al, P, or Si) asymmetric stretching band in the region of 1100  $\text{cm}^{-1}$  is characteristic of the ordered zeolite framework.<sup>4</sup>

The SAPO-37 was prepared without introducing zirconia collapsing upon calcination, forming an amorphous phase due to the framework's susceptibility to water. Fig. 1 shows the powder XRD patterns of both parent SAPO-37 and SAP-37ZR. The XRD patterns of both samples exhibit reflections at  $2\theta$  values of 6.1, 10, 15.5, 18.6, 20.4, and 23.4°, corresponding to the (111), (220), (331), (333), (440), and (533) planes of the faujasite framework, respectively. The SAP-37ZR, obtained by introducing a zirconia source into the as-prepared SAPO-37, was followed by temperature-programmed reduction (TPR) at 550 °C. The resulting SAP-37ZR retains the X-ray reflections characteristic of the SAPO-37 framework. In addition, peaks appear at  $2\theta$  values of 30.4, 34.6, 35.4, 50, 50.4, 59.6, 60.5, 63.3, and 74.8°, characteristic of the tetragonal-zirconia phase ( $t\text{-ZrO}_2$ ).<sup>18</sup> The powder XRD pattern of the zirconia-loaded sample (SAP-37ZR) exhibited a decrease in the intensity of the (111) and (220) reflections, which are characteristic of the supercages of SAPO-37. This observation supports the encapsulation of zirconia within the supercages of SAPO-37. Additionally, the  $2\theta$  values corresponding to SAP-37ZR are shifted toward higher angles compared to the parent SAPO-37, indicating the incorporation of  $t\text{-ZrO}_2$  within the faujasite structure and its condensation on the zeolitic framework surface. The presence of phosphate species in SAPO-37 facilitates the stabilization of tetragonal zirconia within the framework, while the encapsulation of zirconia helps maintain the integrity of the faujasite SAPO-37 framework.

Among the three zirconia polymorphs,  $t\text{-ZrO}_2$  is typically stable above 1200 °C, while the monoclinic phase dominates at lower temperatures. However, the high-temperature tetragonal

phase can be stabilized at lower temperatures by controlling the crystallite size, adding surface impurities, or creating oxygen vacancies through dopants like  $\text{Y}_2\text{O}_3$ .<sup>12</sup> In this study, the hydrogen atmosphere facilitated the removal of organic templates from the faujasite cages, allowing zirconia to occupy the supercages of SAPO-37 in its stabilized tetragonal phase. The encapsulation of  $t\text{-ZrO}_2$  within the SAPO-37 framework enhanced the structural stability, as confirmed by the powder XRD pattern.

The presence of oxygen vacancies in SAP-37ZR was analyzed using temperature-programmed oxidation (TPO) and electron paramagnetic resonance (EPR) spectroscopy. The TPO profile of SAP-37R, SAP-37ZR, and  $t\text{-ZrO}_2$  (Fig. S2, ESI†) displayed a peak below 400 °C, indicating the presence of oxygen vacancies (OV). EPR spectra of both SAP-37R and SAP-37ZR (Fig. 2) showed a sharp signal at  $g = 2.00$ , attributed to electron trapping at the oxygen vacancies.<sup>19</sup> The SAPO-37 developed oxygen vacancies when reduced at high temperature in the presence of hydrogen flow. The presence of oxygen vacancies in the zeolite framework is in agreement with the literature.<sup>20</sup> These oxygen vacancies within the framework help to stabilize  $t\text{-ZrO}_2$ , and the incorporation of zirconia preserves the crystallinity of SAP-37ZR. The presence of  $t\text{-ZrO}_2$  was confirmed by X-ray photoelectron spectroscopy (Fig. S3, ESI†). The Zr 3d spectra exhibited peaks at 181.6 and 184.1 eV, corresponding to the  $3d_{5/2}$  and  $3d_{3/2}$  spin-orbit components, which are characteristic of  $\text{Zr}^{4+}$  in  $t\text{-ZrO}_2$ .<sup>21</sup>

The field emission scanning electron micrographs (Fig. 3) of SAP-37ZR show a distinct octahedral cubic crystal shape, which is similar to the parent as-prepared SAPO-37 (Fig. S4, ESI†) with appreciable crystallinity, characteristic of the faujasite zeolite structure.<sup>5</sup> The uniform cubic particle size is maintained even after TPR treatment at 550 °C, indicating that the faujasite framework of SAPO-37 remains intact, supported by the embedding of zirconia within its channels and cavities. No additional segregated impurities were observed on the surface of SAP-37ZR, further confirming the encapsulation of  $\text{ZrO}_2$  within the SAPO-37 framework. The HR-TEM image of SAP-37ZR (Fig. 4) shows regularly aligned pores, with dark spots (Fig. S5, ESI†) in the channels indicating the uniform distribution of  $t\text{-ZrO}_2$ .

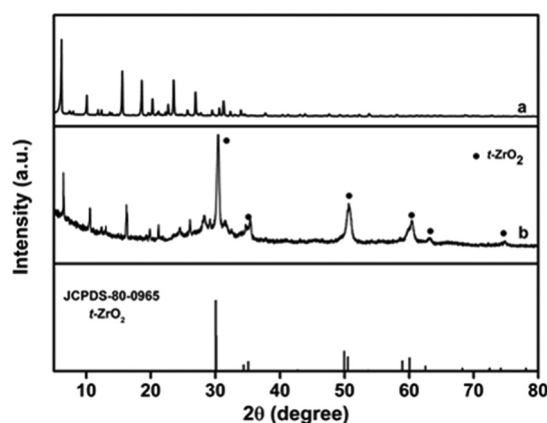


Fig. 1 Powder XRD patterns of (a) SAPO-37 as and (b) SAP-37 ZR.

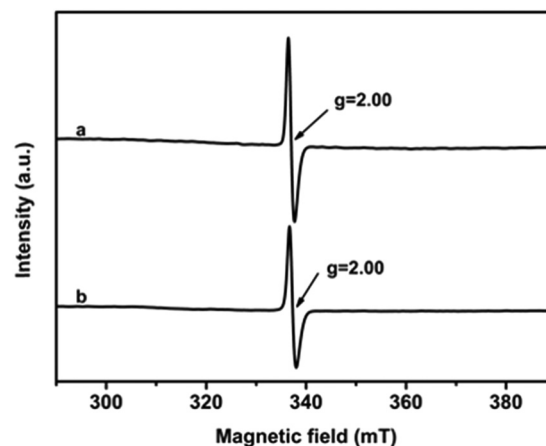


Fig. 2 EPR spectra of (a) SAP-37R and (b) SAP-37ZR.

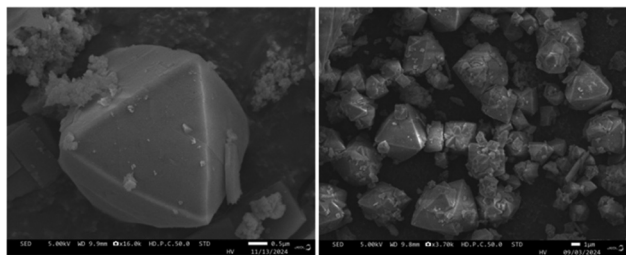


Fig. 3 FE-SEM images of SAP-37 ZR.

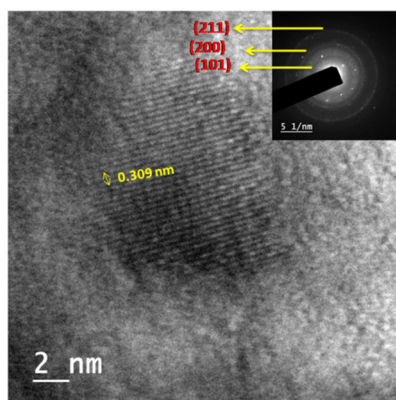


Fig. 4 HR-TEM image and ED pattern of SAP-37 ZR.

The selected area electron diffraction (SAED) pattern confirms the presence of the (101), (200), and (211) planes of  $t\text{-ZrO}_2$ .<sup>18</sup> The chemical environment and elemental coordination of the SAP-37ZR sample were investigated using MAS NMR spectroscopy (Fig. S6, ESI†). The  $^{29}\text{Si}$  MAS NMR spectrum displayed broad resonance peaks at  $-91$  ppm and  $-110$  ppm, corresponding to  $\text{Q}^3 \text{Si}(3\text{Al},1\text{Si})$  and  $\text{Q}^4 \text{Si}(0\text{Al},4\text{Si})$  environments, respectively, indicating the presence of silicon in well condensed states within the framework.<sup>22</sup>

The  $^{27}\text{Al}$  MAS NMR spectrum exhibited a primary signal around  $40$  ppm, attributed to tetrahedrally coordinated aluminium in the SAPO framework. A smaller peak near  $0$  ppm was also observed, associated with hexacoordinated aluminium ( $\text{Al(VI)}$ ), originating from extra-framework aluminium species. The  $^{31}\text{P}$  MAS NMR spectrum of SAP-37ZR showed a strong resonance at  $-27$  ppm, corresponding to tetrahedrally coordinated phosphorus ( $\text{P(4Al)}$ ), which is indicative of a well-crystallized SAPO-37 framework.<sup>23</sup> These findings from the NMR analysis confirm the integrity of the SAPO-37 structure and the presence of zirconia encapsulation without significantly disrupting the framework.

The TG-DTA profiles of the as-prepared zirconia-incorporated SAPO-37 and the samples after temperature-programmed reduction (TPR) are shown in Fig. S7 (ESI†). The as-prepared SAPO-37 with zirconium isopropoxide (wet impregnated) exhibited an overall weight loss of about 27%. The initial 7% weight loss below  $200^\circ\text{C}$  corresponds to the desorption of physisorbed water molecules. The subsequent 20% weight loss above  $200^\circ\text{C}$  is attributed to the decomposition of organic templates, such as

tetrapropylammonium ( $\text{TPA}^+$ ), tetramethylammonium ( $\text{TMA}^+$ ), and residual zirconium isopropoxide.<sup>4</sup> After TPR treatment, the SAP-37ZR sample displayed only a 2% weight loss above  $200^\circ\text{C}$ , indicating that the TPR method effectively removed the organic templates, resulting in the formation of tetragonal zirconia within the channels and cavities of the SAPO-37 framework. Additionally, the predominant desorption of water below  $100^\circ\text{C}$  in SAP-37ZR suggests enhanced accessibility of the zeolite pores, confirming the retention of the porous faujasite structure after zirconia incorporation, which is in agreement with powder XRD, SEM and TEM studies.

In order to assess the surface acidity of the material, temperature-programmed desorption of ammonia ( $\text{NH}_3\text{-TPD}$ ) was conducted, and the results are shown in Fig. S8 (ESI†). The sample exhibited three broad desorption peaks in the ranges of  $100\text{--}200^\circ\text{C}$ ,  $200\text{--}425^\circ\text{C}$ , and  $460\text{--}575^\circ\text{C}$ , corresponding to weak, moderate, and strong acidic sites, respectively. The total acidity was measured as  $0.375 \text{ mmol g}^{-1}$ , which is comparable to that of faujasite-type zeolite materials. The introduction of zirconia increased the acidity of the faujasitic SAPO-37. Nitrogen sorption analysis (Fig. S9, ESI†) revealed a sharp uptake in the  $p/p_0$  range below 0.1, confirming the preservation of the zeolite framework.

The material displayed a surface area of  $119 \text{ m}^2 \text{ g}^{-1}$ , with a pore volume of  $0.231 \text{ cm}^3 \text{ g}^{-1}$ , likely due to the encapsulation of tetragonal zirconia within the channels and cavities of the SAPO-37ZR framework. The as-prepared SAPO-37 exhibited a surface area of  $50 \text{ m}^2 \text{ g}^{-1}$ , which increased to  $119 \text{ m}^2 \text{ g}^{-1}$  for SAP-37ZR, indicating stabilization of the SAPO-37 framework. The thermal stability of SAP-37ZR was evaluated at  $650^\circ\text{C}$ , and the powder XRD pattern of the resulting sample (Fig. S10, ESI†) showed diffraction peaks characteristic of SAPO-37 and  $t\text{-ZrO}_2$ . The well-characterized SAP-37ZR samples were investigated for the synthesis of alkyl levulinate from furfuryl alcohol (FA), and the effect of reactant concentration was analyzed by varying the FA concentration from 2 to 8 mmol (Fig. S11, ESI†). The results indicated similar FA conversion across this concentration range when using 0.05 g of catalyst. Notably, high selectivity for ethyl levulinate (EL) was observed at 4 mmol FA, while a maximum FA conversion of 99%, accompanied by 80% ethyl-furfuryl ether (EFE), was achieved at 8 mmol FA. Reactions with ethanol were conducted both with and without the catalyst over a temperature range of  $120\text{--}190^\circ\text{C}$  (Fig. S12, ESI†). At lower temperatures without the catalyst, the reaction showed poor conversion, with EFE ( $>99\%$ ) as the main product. The use of the SAPO-37ZR catalyst significantly increased FA conversion and resulted in a substantial amount of EL (Table 1). As the temperature increased from  $120$  to  $190^\circ\text{C}$ , FA conversion rose, peaking at 99% (see Table 1). Concurrently, the selectivity for EL increased substantially. At  $190^\circ\text{C}$ , FA conversion reached its maximum with exclusive EL formation (over 99%). At lower temperatures, EFE was the predominant intermediate, which was further converted to EL at higher temperatures.

Although both bare SAPO-37 (SAP-37R) and  $t\text{-ZrO}_2$  showed comparable conversion, their selectivity toward EL was insignificant (Table 1 and Fig. S13, ESI†). The SAPO-37ZR catalyst,

**Table 1** Product distribution at 140 and 190 °C with and without catalyst

	Conversion of FA (%)		Selectivity at 140 °C (%)		Selectivity at 190 °C (%)	
	140 °C	190 °C	EFE	EL	EFE	EL
Without catalyst	13	> 99	> 99	—	94	6
SAP-37ZR	91	> 99	87	13	—	> 99
SAP-37R	64	> 99	95	05	39	61
t-ZrO <sub>2</sub>	16	> 99	92	08	88	22

developed by encapsulating t-ZrO<sub>2</sub> inside the faujasite SAPO-37, facilitates the exclusive formation of ethyl levulinate (EL). The introduction of zirconia increased the acidity of the faujasitic SAPO-37. Furfuryl alcohol molecules were activated by the acidic sites of the tetragonal-ZrO<sub>2</sub>/SAPO-37 composite and then reacted with ethanol molecules to form ethyl levulinate. The acidic sites provided by the tetragonal zirconia enhanced the catalytic activity. To confirm this, we also conducted reactions using sulfated zirconia, which showed good conversion and comparable ethyl levulinate selectivity. To further understand the influence of alcohol on FA conversion, reactions were studied at 170 °C using alcohols of varying chain lengths. Regardless of the alcohol used, the FA conversion exceeded 95%. The major products formed were alkyl furfuryl ether (about 60–90%) and alkyl levulinate (10–40%). When ethanol was the alkylating agent, increasing the reaction temperature to 190 °C facilitated complete FA conversion with exclusive formation of ethyl levulinate (over 99%), which has a potential anti-knocking index. The catalyst demonstrated comparable conversion in recycling studies (Fig. S14, ESI<sup>†</sup>); however, a decrease in conversion was observed, likely due to the chemisorption of reactant molecules on the surface of SAPO-37ZR. To recover its activity, the catalyst was regenerated by high-temperature treatment, which restored complete conversion and exclusive formation of ethyl levulinate (Fig. S13, ESI<sup>†</sup>).

The crystal structure, morphology, and textural properties of the used catalyst were analyzed using powder XRD, field emission scanning electron microscopy (FESEM), thermogravimetric (TG) analysis, and N<sub>2</sub> sorption studies. The powder XRD and FESEM (Fig. S15 and S16, ESI<sup>†</sup>) analyses confirmed the retention of the crystalline structure and morphology of the used catalyst. The observed decrease in surface area of the used catalyst is attributed to the chemisorption of organic species on the framework during the reaction. TGA of the used sample indicated (Fig. S7c, ESI<sup>†</sup>) weight loss of 8%, characteristic of chemisorbed organic moieties, which is responsible for the slight decrease in conversion during recycling studies. In summary, this study presents the first report on a tetragonal zirconia-SAPO-37 faujasite zeolite composite that is synergistically stabilized under TPR conditions. The acidity of the catalyst demonstrates significant potential for the selective conversion of furfuryl alcohol to ethyl-furfuryl ether and ethyl levulinate.

Prof. A. Sakthivel (supervisor): conceptualization, methodology, formal analysis, writing, editing, funding acquisition.

K. K. Shabana, N. P. Nimisha, Dr B. N. Soumya: methodology, formal analysis, data curation, writing, editing.

The authors thank DST-SERB-CRG/2023/001107, and Khad-heejath Shabana, N. P. Nimisha and Dr. Soumya B. Narendranath thank 09/1108(15575)/2022-EMR-I, DST/INSPIRE/03/2019/000097 and KSHCEA3/344/Govt. Kerala-NKPDF/2022 for financial assistance.

## Data availability

The data supporting this article have been included as part of the ESI<sup>†</sup>.

## Conflicts of interest

There are no conflicts to declare.

## References

- P. R. Pujado, J. A. Rabo, G. J. Antos and S. A. Gembicki, *Catal. Today*, 1992, **13**, 113.
- M. Briend, M. Derewinski, A. Lamy and D. Barthomeuf, *Stud. Surf. Sci. Catal.*, 1993, **75**, 409.
- G. N. Kalantzopoulos, F. Lundvall, K. Thorshaug, A. Lind, P. Vajeeston, I. Dovgaliuk, B. Arstad, D. S. Wragg and H. Fjellvåg, *Chem. Mater.*, 2020, **32**, 1495.
- R. Yadav, M. Ahmed, A. K. Singh and A. Sakthivel, *Sci. Rep.*, 2016, **6**, 22813.
- K. K. Shabana, S. B. Narendranath, N. P. Nimisha, N. J. Venkatesha, G. Sheetal and A. Sakthivel, *Chem. Commun.*, 2024, **60**, 8688.
- R. Ma, Y. Zhou, H. Wu, J. Wang, X. Yan, W. Huang and L. Ren, *Inorg. Chem.*, 2024, **63**, 14539.
- Q. Yan, X. Wu, H. Wang, F. Xu, H. Li, H. Zhang and S. Yang, *Coord. Chem. Rev.*, 2024, **502**, 215622.
- L. Ban, D. Wu, D. San, H. Zhou, H. Wang, H. Zhang, C. C. Xu and S. Yang, *ChemSusChem*, 2024, e202401025.
- K. Nikoofar, N. Shaddel and F. Jozi, *Curr. Org. Chem.*, 2024, **28**, 433.
- C. J. Norman, P. A. Goulding and P. J. Moles, *Stud. Surf. Sci. Catal.*, 1994, **90**, 269.
- K. M. Parida and P. K. Pattanayak, *J. Colloid Interface Sci.*, 1996, **182**, 381.
- Z. Zakaria, S. H. Abu Hassan, N. Shaari, A. Z. Yahaya and Y. Boon Kar, *Int. J. Energy Res.*, 2020, **44**, 631.
- W. Zhou, S. Shi, Y. Wang, L. Zhang, Y. Wang, G. Zhang and Y. Wang, *Chem. Cat. Chem.*, 2019, **11**, 1681.
- Y. Wang, T. Yang, F. Liu, T. Zhao, X. Wang and J. Cao, *Microporous Mesoporous Mater.*, 2020, **305**, 110358.
- N. Shimoda, K. Nakayama, K. Kiyota and S. Satokawa, *RSC Adv.*, 2017, **7**, 55819.
- A. Wojtaszek-Gurdak and M. Ziolk, *RSC Adv.*, 2015, **5**, 22326.
- G. M. G. Maldonado, R. S. Assary, J. A. Dumesic and L. A. Curtiss, *Energy Environ. Sci.*, 2012, **5**, 8990.
- F. Chen, L. Huang, Z. Zhong, G. J. Gan, S. M. Kwan and F. Kooli, *Mater. Chem. Phys.*, 2006, **97**, 162.
- S. Wu, M. Y. Manuputty, Y. Sheng, H. Wang, Y. Yan, M. Kraft and R. Xu, *Small Methods*, 2021, **5**, 2000928.
- I. Balint, M. A. Springuel-Huet, K. I. Aika and J. Fraissard, *Phys. Chem. Chem. Phys.*, 1999, **1**, 3845.
- A. Gulino, S. La Delfa, I. Fragala and R. G. Egdel, *Chem. Mater.*, 1996, **8**, 1287–1291.
- N. P. Nimisha, S. B. Narendranath and A. Sakthivel, *Chem. Commun.*, 2024, **60**, 1480.
- C. Blackwell and R. Patton, *J. Phys. Chem.*, 1988, **92**, 3965.